Response Properties of Magnesium Doped Strontium Titanate Electrorheological Composite Hydrophilic Elastomers Based on Different Morphologies

Shu-Juan Gao *, Lin-Zhi Li, Peng-Fei Han, Ling Wang, Feng Li, Tan-Lai Yu, Yan-Fang Li *

Posted Date: 12 June 2024

doi: 10.20944/preprints202406.0849.v1

Keywords: Mg-doped strontium titanate; morphology; electrorheological composite hydrophilic elastomers

 doi:10.20944/preprints202406.0849.v1

Article

Response Properties of Magnesium Doped Strontium Titanate Electrorheological Composite Hydrophilic Elastomers Based on Different Morphologies

Shu-Juan Gao [1,2,*], Lin-Zhi Li [1,2], Peng-Fei Han [3], Ling Wang [1], Feng Li [1], Tan-Lai Yu [1,2] and Yan-Fang Li [1,*]

[1] Department of Chemical and Materials Engineering, Lyuliang University, Lishi Shanxi 033001, China
[2] Institute of New Carbon-based Materials and Zero-carbon and Negative-carbon Technology, Lyuliang University, Lishi Shanxi 033001, China
[3] Institute of Teacher Education, Taiyuan Normal University, Taiyuan 030006, China; 201722801006@email.sxu.edu.cn (P.-F.H.)
* Correspondence: shujuangao@llu.edu.cn (S.-J.G.); 20131017@llu.edu.cn (Y.-F.L.)

Abstract: As a member of smart materials, electrorheological elastomers (EREs) formed by pre-treating active electrorheological particles are attracting more and more attention. In this work, four Mg-doped strontium titanate particles with spherical, dendritic, flake-like and pinecone-like morphorlogies were obtained by hydrothermal and low-temperature co-precipitation. XRD, SEM, Raman and FT-IR were used to characterize the obtained products. The results showed that the sizes of Mg-doped strontium titanates are about 1.5–2.0 μm, and the phase structure are dominated by cubic crystal. These Mg-doped strontium titanates were dispersed in a hydrogel composite elastic medium. Then, Mg-doped strontium titanate/glycerol/gelatin electrorheological composite hydrophilic elastomers were obtained with or without electric field. The electric field response properties of Mg-doped strontium titanate composite elastomers were investigated. It concluded that dendritic Mg-doped strontium titanate composite elastomers is high-performance EREs. And the maximum value of energy storage modulus of Mg-doped strontium titanate composite elastomers has achieved 8.70 MPa. This high electrorheological performance of the products is helpful for their applications in vibration control, force transducers, smart structures, dampers, and other fields.

Keywords: Mg-doped strontium titanate; morphology; electrorheological composite hydrophilic elastomers

1. Introduction

Electrorheological (ER) materials have exhibited bright prospects in the area of new energy and new materials, such as the actuators, valve devices, artificial muscles, flexible skin, etc [1–9]. It's all due to their advantages of controllability, reversibility, electric field response (EFR)and other electrorheological properties. Electrically and magnetically motivated smart composites include electrorheological fluids, magnetorheological fluids, electrorheological hydrogels, magnetorheological elastomers, and so on. The rheology or animation viscoelasticity of such smart composites can be adjusted in real time and reversibled rapidly by electric or magnetic field. So, it is widely applied in vibration damping, variable rigidity control, and flexible robotics. The viscoelastic response properties of gels are quite sensitive to internal structural changes of materials, and thus the rheological behaviors are crucial for better understanding flow properties and mechanical properties of ER materials.

Electrorheological elastomers are composite elastomers obtained by dispersing electrolyte particles of dispersed phase into an interpenetrating network (IPN) of macromolecular compound [10–16]. These smart soft materials have obvious stimulation response to an applied electric field based on electrorheological fluids. Since EREs combine the advantages of both electrorheological fluid and elastomer, it can overcome the shortcomings of easy to precipitate and weak stability for

 doi:10.20944/preprints202406.0849.v1

ordinary hydrogel. The dispersed particles in ERE would form specific anisotropic structures under electric field, which caused mechanical modulus changed significantly and showed potential for the application in electric field-modulated wave-absorbing material [17–20]. However, high ERE rheological activity for close level of electrorheological fluid has become a major challenge.

Recently, Shiga and his coworkers prepared composite hydrogels by dispersing cobalt polyacrylate, a semiconducting polymer particle, in silica gel via cross-linking polydimethylsiloxane polymerization [21]. In their work, the energy storage shear modulus and loss modulus of the hydrogel increased and the loss angular tangent changed with an applied DC electric field at room temperature [22]. Hanaoka and coworkers used hydrogenated methylsiloxane and ethylene methylsiloxane prepolymers containing unsaturated groups to obtain a continuous phase polymer after a silica-hydrogenation polymerization reaction. In order to prepare a continuous phase with suitable elasticity and conductivity, the researchers chose prepolymers with certain physical parameters. And the magnitudes of modulus of whole gel were modulated by gelation temperature and time [23]. Shaw et al. obtained a series of silicone rubbers with different compositions by cross-linking two siloxanes in the presence of platinum catalysts [24]. He and coworkers prepared speed-induced extensibility elastomers (SIE) with good resilience and high toughness [25]. The thermoplastic elastomers have unique properties of positive correlation between strain rate and elongation of rupture, modulus and strength at room temperature. The obtained elastomers exhibited excellent resiliency, crack resistance, and self-healing properties. Joseph designed an electrorheological hydrogel actuator for a rehabilitation robotic, which could apply to late-stage stroke treatment [26]. The actuator has a simple structure, short response time and low inertia, which is conducive to the miniaturization and domestication of rehabilitation robots. The results offered the possibility for the application of electrorheological hydrogels in smart organs. All the above studies showed that the composition and structure of dispersed phase play an important role in influencing the electrorheological properties of hydrogels [27–32].

Based on it, the problems related to hydrophilic EREs have become a new hotspot in the field of electrorheological (ER) fluid materials. ER particles and EFR particles have a common characteristic that their electrical performance depends on the mode of polarization of particles under electric field [11,13,16]. The ER properties are usually as good as the EFR properties for the easily polarizable particles. Particles with good EFR properties are the prerequisite for qualified ER particles. Thus, selecting a high dielectric constant dispersed phase is crucial for improving the EFR. Cubic magnesium doped strontium titanate is the ideal dispersed phase material for its high dielectric constant and strong ferroelectric response [33–35]. Magnesium doped strontium titanate (Mg-STO) has gathered the excellent properties of both magnesium titanate and strontium titanate. It is expected that Mg-doped strontium titanate particles may have a stronger EFR due to the tendency of cubic strontium titanate polarization spontaneously along the c-axis [36]. The polarity of $SrTiO_3$ is modified by doping with different amounts of Mg, which in turn can improve its dielectric properties. Up to now, the relationship between the morphology and EFR performance of Mg-doped $SrTiO_3$ has rarely been investigated. Therefore, the preparation of Mg-doped $SrTiO_3$ with different morphologies and the study of its electric field response properties are of great significance in both theoretical and practical applications.

In this contribution, we have prepared four different morphologies of Mg-doped strontium titanate by hydrothermal and low-temperature co-precipitation methods. Then the effect of morphology on EFR performance of Mg-doped $SrTiO_3$ are discussed to obtain high-performance dendritic Mg-doped $SrTiO_3$ composite elastomers.

2. Experimental Section

2.1. Preparation of Mg-STO

2.1.1. Preparation of Spherical and Pinecone Shaped Mg-STO

Spherical and pinecone shaped Mg-doped $SrTiO_3$ are labeled M1 and M4. They are prepared by a one-step hydrothermal method using titanium tetrachloride as the titanium source, sodium

 doi:10.20944/preprints202406.0849.v1

hydroxide as the mineralizing agent, and dilute hydrochloric acid as the hydrolysis inhibitor, separately [37]. The morphology of M1 is spherical, which is monodisperse and regular, with smooth surface and size about 1.8 μm (*vide infra*). M4 has a pinecone-shaped micro-nanostructure, which is composed of dozens of nano-sized spheres with the size distribution of 2.0 μm (*vide infra*).

2.1.2. Preparation of Dendritic and Flake-Like Mg-STO

According to the literature [38], Mg-doped $SrTiO_3$ with dendritic and flake-like morphologies were prepared via a low temperature co-precipitation method through regulating the pH of $SrMg_xTi_{1-x}O(C_2O_4)_2$ precursor solution. In contrast to the literature, $Sr(OH)_2$ and $Mg(NO_3)_2$ were added to substituted B-site, according to the solid solubility limit of about 2.00 mol%, i.e., $n[Sr^{2+}]:n([Mg^{2+}]+[Ti^{4+}]) = 1.00$, $n[Mg^{2+}]:n([Mg^{2+}]+[Ti^{4+}]) = 0.02$. Remarkably, dendritic Mg-doped $SrTiO_3$ M3 was obtained from pH = 4.97 $SrMg_xTi_{1-x}O(C_2O_4)_2$ precursor solution succeeding. Flake-like Mg-doped $SrTiO_3$ M4 was followed by $SrMg_xTi_{1-x}O(C_2O_4)_2$ precursor solution with pH = 6.87. The final products were then calcined in a muffle furnace (vacuum) at 700 °C for 4 h.

2.2. Preparation of Electrorheological Composite Hydrophilic Elastomers

A certain amount of Mg-doped $SrTiO_3$ was ground, homogenized, and dispersed in a gelatin/glycerol/water at 65 °C in a water bath. The cross-linking agent glutaraldehyde was added quickly and placed in two plexiglas boxes (40×20×3 mm^3). The gel was applied in the presence or absence of an external DC electric field (1.2 kV/mm) for 30 min at 65 °C and moved to room temperature for 20 min. Finally, the gelation was kept for 7 h to obtain the elastomer without the external electric field. The Mg-doped $SrTiO_3$ gelatin/glycerol hydrophilic elastomers were prepared referred to A-elastomer (0.00 kV/mm) and B-elastomer (1.20 kV/mm), respectively [38–40]. The energy-storage modulus of composite elastomers were tested by dynamic viscoelastic spectroscopy and the energy-storage modulus/frequency curves were obtained in multi-frequency modes. The relationship between the hardness variation of composite elastomer and morphology of Mg-STO is explored according to the curves [38,41]. Thus, the exotic response properties of Mg-STO with different morphologies to applied electric fields were further investigated [37].

2.3. Characterizations

The morphologies and structures of products were studied using a scanning electron microscope (SEM, Questar, 450 Quanta™) and a Fourier transform infrared spectrometer (FTIR, EQUIOX55, in the range of 4000–500 cm^{-1}). X-ray diffraction spectra was recorded by a diffractometer (XRD, Rigaku D/MAX-2550, λ = 1.5512 Å) of Cu/Kα radiation. The elemental composition of the product was detected by an ICP-AES tester. The contact angle of Mg-STO was measured by OCA20 video optical contact angle tester. The pH of solution was checked by German Sedovis PB-10 acidity meter. And the dielectric properties were obtained by HP4284A dielectric constant tester. The energy-storage modulus of composite elastomer was eventually measured by a Q800DMA dynamic viscoelastic spectrometer.

3. Results and Discussion

3.1. ICP Analyses of Mg-STO

Figure 1(a, b) show the SEM images of spherical samples. They are spherical with regular shape and size about 1.8 μm. The single dendritic Mg-STO is in the form of elongated long rods, and the length-to-diameter ratio of this "microrod" is large (Figure 1(c, d)). The diameter of dendritic $SrMg_xTi_{1-x}O_3$ is about a few nanometers, and the length is only ~1 μm. Each branch consists of many small strips. The microstructure of the flake Mg-STO are observed from Figure 1(e, f), which consists of a group of sheet cells arranged haphazardly together. The particle size ranges from 5 μm to 20 μm. Figure 1(g, h) show the Mg-STO with a morphology similar to pinecone with micrometer-sized particles formed by dozens of nanometer-sized balls [36]. That is, the micro-nano structure, which is constructed by combining nano-sized matrix units with each other. It's also the case that the

 doi:10.20944/preprints202406.0849.v1

protruding spheres of about 300 nm in Figure 1(h) synergistically build micrometer-sized particles. The final micro-nanostructure reaches 2.0 μm. The elemental composition of samples M1-M4 were determined by ICP. Ultimately, the chemical formulae of samples M1-M4 are $Sr_{1.10}Mg_{0.03}Ti_{1.00}O_3$, $Sr_{1.01}Mg_{0.02}Ti_{0.98}O_3$, $Sr_{1.02}Mg_{0.02}Ti_{0.98}O_3$, and $Sr_{1.07}Mg_{0.02}Ti_{0.99}O_3$, respectively (see Table 1).

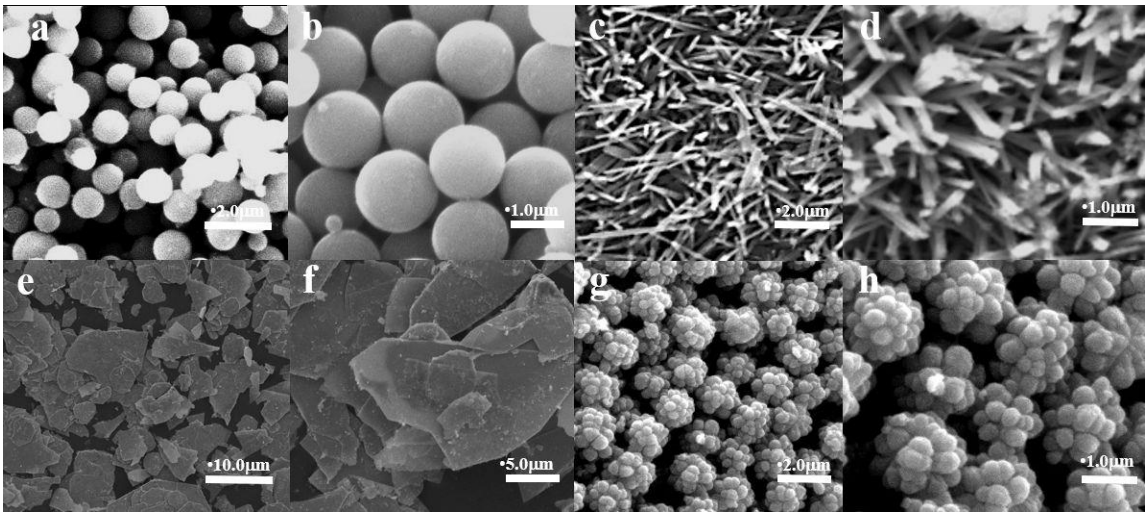

Figure 1. SEM patterns of Mg-STO (a, b) spherical, (c, d) dendritic, (e, f) flake-like, and (g, h) pinecone-like.

Table 1. ICP analyses data of Mg-STO.

Sample	Sr/mol	Mg/mol
M1	1.095	0.030
M2	1.013	0.017
M3	1.021	0.023
M4	1.071	0.022

3.2. XRD and Roman Analyses of Mg-STO

The X-ray diffraction (XRD) patterns of M1-M4 are shown in Figure 2. It can be clearly seen that the characteristic diffraction peaks of cubic Mg-STO have been completely formed. The diffraction peaks of four products are located at 31.35~32.42°, 22.1°, 31.5°, 38.7°, 45.1°, 50.7~56.0°, and 66°, which correspond to the seven characteristic peaks in the Mg-doped $SrTiO_3$ standard card (JCPDS No. 073-0661). The diffraction peaks of four samples were almost identical to standard peaks, except for weak shifts at [110] and [211]. It suggests the partial substitution of Ti^{2+} by Mg^{2+} in the $SrTiO_3$. Raman techniques was employed to further characterize the crystalline phase of Mg-STO accurately. The 305 cm^{-1} neighborhood band corresponds to the Bl vibrational mode in Figure 3 [42]. It is the characteristic band of tetragonal Mg-STO. The 305 cm^{-1} band begin to appear one step in dendritic and spherical patterns, which indicates tetragonal structure. In contrast, the tetragonal characteristic peaks are weak or disappear in the flake-like and pinecone-like patterns. It can be attributed to the fact that the amount of tetragonal structure is tiny and almost undetectable. It also means the products have no Raman activity (i.e., no diffraction peaks corresponding to the products of tetragonal phases appeared in Raman patterns) and hence they belong to the cubic phase. The four Mg-STO are dominated by cubic-perovskite phase structure, which is consistent with their XRD observations. The Raman activity intensity of four samples is in the order of spherical > pinecone-like > dendritic > flake-like. A polarization occurs in the interior of the crystal where Mg^{2+} and Sr^{2+} ionic layers alternate along the [001] direction, creating microelectric domains. Subsequently, a dipole moment is generated, which shifts the polarity of particles. But this polarity shifts only occur in local regions, therefore this phenomenon is known as lattice structure micro-disturbances. It hardly affects the basic structure of the crystals. That is why Mg-doped STO differ in microstructure from STO with a classical perovskite structure.

Preprints.org (www.preprints.org) | NOT PEER-REVIEWED | Posted: 12 June 2024 doi:10.20944/preprints202406.0849.v1

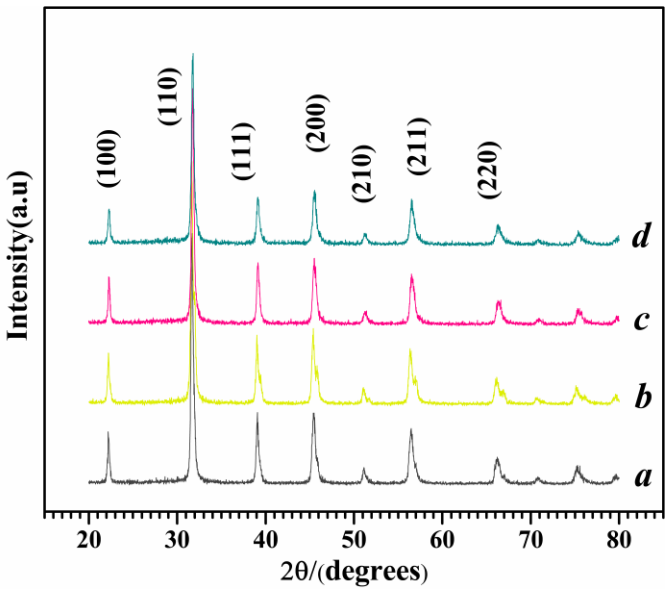

Figure 2. XRD patterns of Mg-STO (a) spherical, (b) dendritic, (c) flake-like, and (d) pinecone-like.

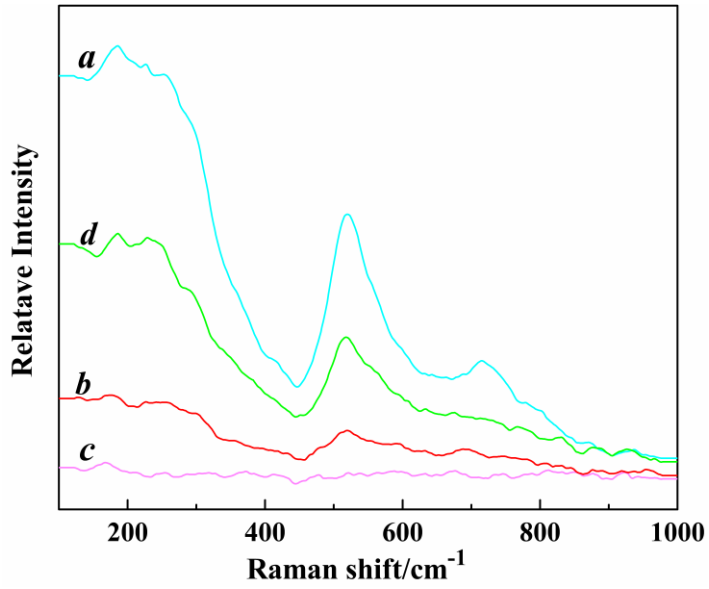

Figure 3. The Raman patterns of different morphologies of Mg-STO (a) spherical, (b) dendritic, (c) flake-like, and (d) pinecone-like.

3.3. The FI-IR Analyses of Mg-STO

The stretching vibrations v(O–H) of O–H broadband at 3438 cm^{-1} for Mg-STO is illustrated in Figure 4 [43]. A spectral band near 1627 cm^{-1} is assigned to the coordinated water of H–O bending vibrational [44]. The two weak absorption peaks appearing near 2900 cm^{-1} are the C–H stretching vibrations. Two sharp peaks at 1300~1100 cm^{-1} are the evidences of C–H bending vibration located in alkyl chain, suggesting the presence of minor residual ethanol on the surface of Mg-STO. The FTIR results show that the Ti–O stretching vibration bands are around 400~1000 cm^{-1} in the products. In contrast to the normal 612 cm^{-1} band, this broadband is considered to be a stretching mode of Ti–O bond in TiO_2. The bands at 583 cm^{-1} and 437 cm^{-1} are generated by the Ti–O stretching vibrations in the four Mg-STO. The intensity and sharpness of these absorption bands increase dramatically, indicating that all four products are pure Mg-STO crystals.

 doi:10.20944/preprints202406.0849.v1

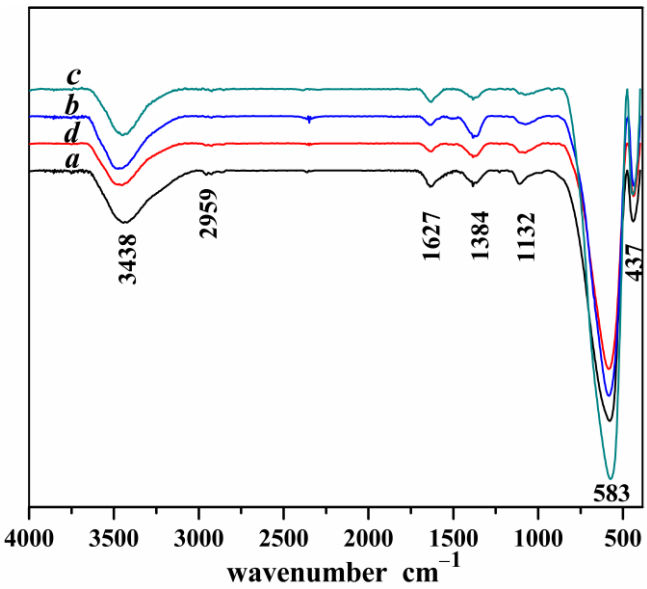

Figure 4. FT-IR diagrams of four kinds of Mg-STO (a) spherical, (b) dendritic, (c) flake-like, and (d) pinecone-like.

3.4. The Hydrophilicity Measurement of Mg-STO

The infiltration on the surface of M1-M4 particles was measured by sessile drop method under video-based optical contact angle meter. The current test was performed on Mg-doped STO thin film samples. It was prepared as follows: a suspension of dried Mg-STO in ethanol was prepared by grinding and ultrasonic dispersion. A clean glass slide was then inserted vertically and slowly pulled out at a certain speed (5 cm/s). Finally, they were dried at room temperature and the process was repeated three times. Then Mg-STO films were formed on the surface of slide. The 3 μL of water was dropped into the film using a fine-tuned syringe. The contact angle between waterdrop and film could be measured. The contact angles between different morphologies of Mg-doped STO and water are shown in Figure 5. Unsurprisingly, the contact angles of M1-M4 with water are 32.7°, 13.9°, 7.4°, and 21.6°, respectively. They are all less than 35.0°, indicating that they are superhydrophilic materials with excellent dispersion and good compatibility in water [45–47].

The hydrophilicity of four Mg-STO is in the order of flake-like > dendritic > pinecone-like > spherical. According to the rule of surface roughness on contact angle of microstructures, the larger the surface roughness, the smaller the contact angle. The order of roughness of the four products is flake-like > dendritic > pinecone-like > spherical in turn. Therefore, the contact angle of flake-like Mg-STO is the smallest and then it has the maximum hydrophilicity. We also calculated the surface energies of four Mg-STO. The surface energy test was performed using water and diiodomethane as titrant. The dispersive and polar components of surface energy for water/diiodomethane were 22.1/48.50 and 50.65/2.30 mN/m, respectively. The surface energies of flake-like, dendritic, pinecone-like and spherical Mg-STO were calculated to be 72.41, 71.24, 68.81, and 64.07 mN/m in the T-Yong equation [48]. Flake-like Mg-STO has the largest surface energy, in line with its maximum hydrophilicity. The larger surface energy, the stronger wettability of liquid owing to the intermolecular van der Waals and Coulomb forces. And the larger the proportion of the polar part in the dispersive and polar energies, the stronger its adsorption capacity.

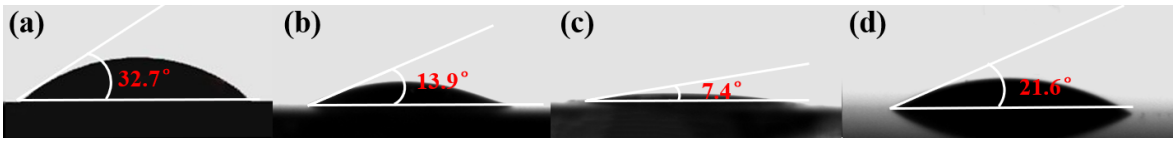

Figure 5. Contact angles of water drops (3 μL) on the Mg-STO with different shapes (a) spherical, (b) dendritic, (c) flake-like, and (d) pinecone-like.

 doi:10.20944/preprints202406.0849.v1

3.5. The Dielectric Measurement of Mg-STO

The dielectric spectra of Mg-STO ER fluids from 20 Hz to 1 MHz frequency were experimentally investigated in order to study the relationship between their structures and dielectric properties (Figure 6). The dried Mg-STO was dispersed into silicone oil (η = 50 mPa·s at 25 °C) with grinding and ultrasonic dispersion. The dielectric mass spectra of samples were then measured by current analyzer with 1 V bias potential. Figure 6 shows the frequency dependence of real part (ε′) of complex dielectric constant. It can be seen that room temperature dielectric constants of all products were not significantly influenced by the fluctuation of frequency (*only slightly decreases*) [49]. The order of dielectric constant magnitude for four products is dendritic > flake-like > pinecone-like > spherical. And each has a maximum dielectric constant (6.15, 5.78, 3.49, and 3.09) at certain frequency (20, 20, 25, and 20 Hz). We speculated that the movement of crystal dipoles becomes relatively easy under low DC voltage electric field. When the particle size is determined, the wider the interplanar crystal spacing, the greater the tetragonal distortion of unit cells. The interplanar crystal spacing of dendritic Mg-STO is larger than other three morphologies of samples, therefore the dielectric constant of dendritic Mg-STO reaches the maximum value [50].

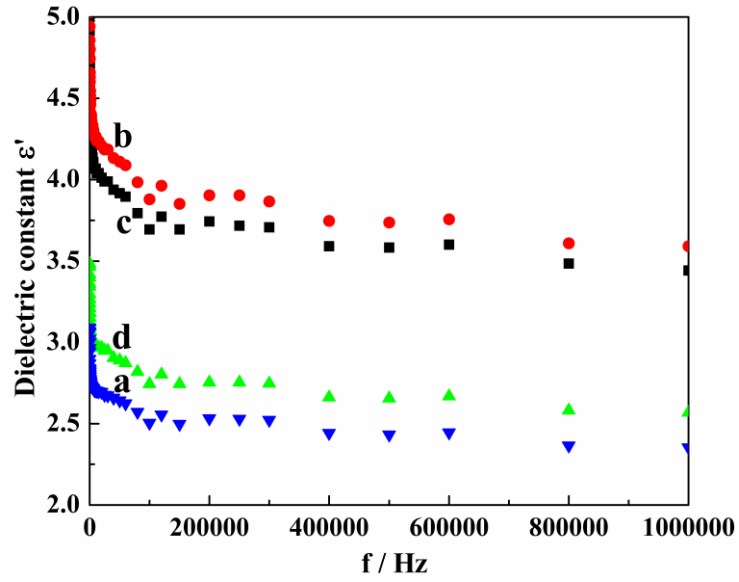

Figure 6. Dielectric spectra of the as-made samples (a) spherical, (b) dendritic, (c) flake-like, and (d) pinecone-like.

3.6. The Analyses of EFR Performance of Mg-STO

The energy storage modulus of materials is the amount of elastic energy stored per unit volume within the elastic deformation ranges of the material. It is one of the most important metrics for the elastic properties of elastomers. The energy storage modulus reflects the degree of elastic deformation of material with stress, which can also be understood as the degree of softness or rigidity of elastomer. Obviously, the energy storage modulus is closely related to elastic modulus of elastomer. The elastic modulus is the ability to restore a material to its original state with elastic deformation. And it is the physical quantity that describes the stiffness of elastomer. Typically, the energy storage modulus is half the modulus of elasticity, which is equal to the modulus of elasticity multiplied by half the coefficient of volumetric elasticity of elastomer.

The energy-storage modulus of A- and B-elastomers (Mg-STO/glycerol/gelatin hydrogel elastomers) versus frequency at a fixed strain of 0.01% are shown in Figure 7. The values of storage modulus for each elastomer exhibit insignificant variations with increasing frequency. Figure 7 a and a' represent elastomers without and with applied electric field, respectively, which do not contain dispersed particles. Figure 7 b(b')~e(e') represent composite elastomers with and without electric field, respectively, where 1.0 wt% of M1-M4 were added. Figure 7 a and a' almost overlapped,

 doi:10.20944/preprints202406.0849.v1

indicating that the pure gelatin/glycerol hydrogel elastomer had no obvious response performance without electric field. The curves b(b')~e(e') are located above a, a', i.e., the energy-storage modulus of elastomer contained Mg-STO particles is larger than pure elastomer at the same frequency. Remarkably but not surprisingly, the hardness of composite elastomer becomes larger due to the filling of Mg-STO. In addition, the modulus/frequency curves of b', c', d', and e' of B-elastomers are all above the curves b, c, d, and e of A-elastomers. It means that the resilience of B-elastomers are greater than A-elastomers, demonstrating the significant response performance of M1-M4.

It is assumed that the dispersion particles are randomly distributed in the elastomer when there is no electric field present during the gelation process. Here the Mg-STO only has a filling effect. Following this, the structure of the elastomer obtained is isotropic. However, the polarized Mg-STO could form chain or columnar microstructure in the elastomer under an applied electric field. This gives the elastomer enhanced compressive properties and increased hardness [20,24,37,51]. Furthermore, we found that the spacing $d_{cc'}$ of curves c and c' is larger than that of dd', ee', and bb' ($d_{cc'} > d_{dd'} > d_{ee'} > d_{bb'} > d_{aa'}$; Figure 7, right panel). The larger gap of energy-storage modulus/frequency curves implies the better response behavior in dispersed particles under an electric field. Consequently, there exists a line of variation "high degree of polarization of the dispersed particles—regular and ordered aggregation in the electric field—increasing hardness of electrorheological composite elastomers—increasing difference of hardness between A- and B-elastomers" [37,38,52,53].

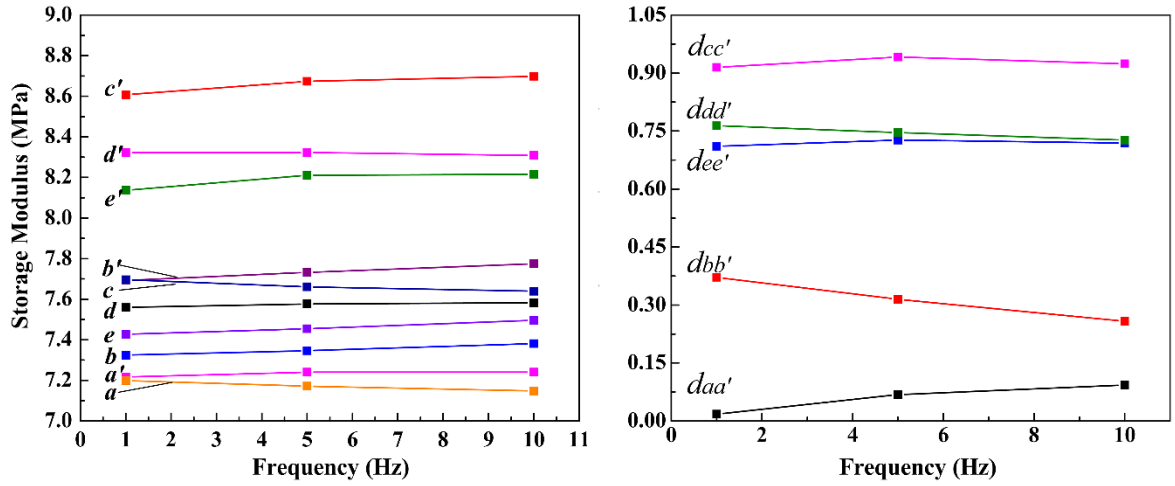

Figure 7. The energy storage-modulus/frequency graphs of composite elastomers with different Mg-STO under electric field (a)~(e) 0.0 kV/mm, (a')~(e') 1.2 kV/mm. Moreover, a and a': without Mg-STO; b and b': with spherical Mg-STO; c and c': with dendritic Mg-STO; d and d': with flake-like Mg-STO; e and e': with pinecone-like Mg-STO.

4. Conclusions

In this study, four $SrMg_xTi_{1-x}O_3$ with different morphologies (spherical, dendritic, flake-like and pinecone-like) were successfully prepared via two methods: one-step hydrothermal method and low-temperature co-precipitation method. They are different in composition, surface morphology, surface hydrophilicity and dielectric properties. It is found that the rough surface morphology of cubic Mg-doped $SrTiO_3$ affects their surface hydrophilicity. And the particles with higher length-diameter ratio exhibit better dielectric properties. The prepared four products were dispersed in hydrogel composite elastomer medium. Then the EFR properties of the obtained Mg-STO/glycerol/gelatin composite elastomers were investigated. In conclusion, the high cubic structure, excellent dielectric properties and super hydrophilicity of dendritic Mg-doped $SrTiO_3$ particles have a synergistic effect on the electric field response performance of electrorheological composite hydrophilic elastomers. We confirmed the molecular formula of M1–M4 samples were $Sr_{1.10}Mg_{0.03}Ti_{1.00}O_3$, $Sr_{1.01}Mg_{0.02}Ti_{0.98}O_3$, $Sr_{1.02}Mg_{0.02}Ti_{0.98}O_3$, and $Sr_{1.07}Mg_{0.02}Ti_{0.99}O_3$. Four kinds of magnesium doped strontium titanate are all super-hydrophilic materials by measuring contact angle, and all contact angles less than 33.0°. The

 doi:10.20944/preprints202406.0849.v1

EFR properties of samples are dendritic > flake-like > pinecone-like > spherical, which are consistent with the arrangement of dielectric constants. Eventually, it was determined that the maximum values of energy storage modulus and dielectric constant have achieved 8.70 MPa and 6.15.

Author Contributions: Conceptualization, S.-J.G. and Y.-F.L.; methodology, S.-J.G. and P.-F.H.; validation, L.-Z.L. and L.W.; investigation, F.L., T.-L.Y. and S.-J.G.; writing—original draft preparation, S.-J.G.; writing—review and editing, S.-J.G. and Y.-F.L. All authors have read and agreed to the published version of the manuscript.

Funding: This work was supported by the National Natural Science Foundation of China (22173053), the Natural Science Foundation of Shanxi Province (201801D121103 and 202303021212289), the Shanxi "1331" Project, and Lvliang City high-level scientific and technological talents project (2023RC14).

Conflicts of Interest: The authors declare no conflict of interest.

References

1. Lavalle, P.; Voegel, J.C.; Vautier, D.; Senger, B.; Schaaf, P. Dynamic aspects of films prepared by a sequential deposition of species: Perspectives for smart and responsive materials. *Adv. Mater.* **2011**, 23, 1191–1221.
2. Yarimaga, O.; Jaworski, J.; Yoon, B.; Kim, J.M. Polydiacetylenes: Supramolecular smart materials with a structural hierarchy for sensing, imaging and display applications. *Chem. Commun.* **2012**, 48, 2469–2485.
3. Niu, X.; Zhang, M.; Wu, J.; Wen, W.; Sheng, P. Generation and manipulation of "smart" droplets. *Soft Matter.* **2009**, 5, 576–581.
4. Ohko, Y.; Tatsuma, T.; Fujii, T.; Naoi, K.; Niwa, C.; Kubota, Y.; Fujishima, A. Multicolour photochromism of TiO_2 films loaded with silver nanoparticles. *Nat. Matter.* **2003**, 2, 29–31.
5. Varga, Z.; Filipcsei, G.; Zrinyi, M. Magnetic field sensitive functional elastomers with tuneable elastic modulus. *Polymer* **2006**, 47, 227–233.
6. Adrian Koh, S.J.; Li, T.-F.; Zhou, J.-X.; Zhao, X.-H.; Hong, W.; Zhu, J.; Suo, Z.-G. Mechanisms of large actuation strain in dielectric elastomers. *J. Polym. Sci.* **2011**, 49, 504–515.
7. Chakraborti, P.; Karahan Toprakci, H.A.; Yang, P.; Spigna, N.D.; Franzon, P.; Ghosh, T. A compact dielectric elastomer tubular actuator for refreshable braille displays. *Sens. Actuators A*, **2012**, 179, 151–157.
8. Xia, H.; Takasaki, M.; Hirai, T. Actuation mechanism of plasticized PVC by electric field, *Sens. Actuators A*, **2010**, 157, 307–312.
9. Gao, L.-X.; Zhan, L.-J.; Liu, W.; Zhang, Y.-L.; Xie, Z.-Y.; Ren, J. Preparation and electro responsive properties of Mg-doped $BaTiO_3$ with novel morphologies. *J. Mater. Sci-Mater. El.* **2019**, 30, 12107–12112.
10. Hao, L.; Shi, Z.; Zhao, X. Mechanical behavior of starch/silicone oil/silicone rubber hybrid electric elastomer. *React. Funct. Polym.* **2009**, 69, 165–169.
11. Li, Y.-Q.; Li, X.-N.; Chen, C.; Su, Z.-G.; Ma, G.-H.; Yu, R. Sol-gel transition characterization of thermosensitive hydrogels based on water mobility variation provided by low field NMR. *J. Polym. Res.* **2017**, 24, 25.
12. Dashtimoghadam, E.; Mirzadeh, H.; Taromi, F.A.; Nyström, B. Thermoresponsive biopolymer hydrogels with tunable gel characteristics. *RSC Adv.* **2014**, 4, 39386–39393.
13. Dong, X.-F.; Niu, C.-G.; Qi, M. Enhancement of electrorheological performance of electrorheological elastomers by improving TiO_2 particles/silicon rubber interface. *J. Mater. Chem. C* **2016**, 4, 6806–6815.
14. Chen, J.; Li, H.-F.; Han, H.-J.; Sun, R.-Y.; Xie, M.-R. Multiple polarizations and nanostructure of double-stranded conjugated block copolymer for enhancing dielectric performance. *Mater. Lett.* **2017**, 208, 95–97.
15. Liu, W.; Xie, Z.-Y.; Lu, Y.-P.; Gao, M.-X.; Zhang, W.-Q.; Gao, L.-X. Fabrication and excellent electroresponsive properties of ideal PMMA@$BaTiO_3$ composite particles. *RSC Adv.* **2019**, 9, 12404–12414.
16. Xue, B.-X.; He, F.; Zhao, X.-P.; Yin, J.-B. Electro-responsive electrorheological effect and dielectric spectra analysis of topological self-crosslinked poly (ionic liquid)s. *Eur. Polym. J.* **2022**, 170, 111160.
17. Gao, L.-X.; Gao, S.-J.; Wei, W.-X.; Zhang, W.-Q. Morphology modification of micron-sized barium strontium titanate by hydrothermal growth. *J. Mater. Sci-Mater. El.* **2015**, 26, 1354–1362.
18. Dong, W.-J.; Li, X.-Y.; Yu, J.; Guo, W.-C.; Li, B.-J.; Tan, L.; Li, C.-R.; Shi, J.-J. Porous $SrTiO_3$ spheres with enhanced photocatalytic performance. *Mater. Lett.* **2012**, 67, 131–134.
19. Huang, Y.; Zhao, X.-P.; Wang, L.-S.; Luo, C.-R. Tunable left-handed metamaterial based on electrorheological fluids. *Prog. Nat. Science-Mater.* **2008**, 18, 907–911.
20. Tang, H.; Zhao, X.-P.; Wang, B.-X.; Zhao, Y. Response characteristics of a viscoelastic gel under the co-action of sound waves and an electric field. *Smart Mater. Struct.* **2006**, **15**, 86–92.
21. Chen, H.; Cheng, R.; Zhao, X.; Zhang, Y.; Tam, A.; Yan, Y. An injectable self-healing coordinative hydrogel with antibacterial and angiogenic properties for diabetic skin wound repair. *NPG Asia. Mater.* **2019**, 11, 1427–1429.

 doi:10.20944/preprints202406.0849.v1

22. Shiga, T.; Ohta, T.; Hirose, Y.; Okada, A.; Kurauchi, T. Electroviscoelastic effect of polymeric composites consisting of polyelectrolyte particles and polymer gel. *J. Mater. Sci.* **1993**, 28, 1293–1299.
23. Hanaoka, R.; Takata, S.; Nakazawa, Y.; Fukami, T.; Sakurai, K. Effect of electric field on viscoelastic properties of a disperse system in silicone gel. *Electr. Eng. Jpn.* **2003**, 142, 1–9.
24. An, Y.; Shaw, T.M. Actuating properties of soft gels with ordered iron particles: basis for a shear actuator. *Smart Mater. Struct.* **2003**, 12, 157–163.
25. Chen, H.-M.; Koh, J.-J.; Long, C.-J.; Liu, S.-Q.; Shi, H.-H.; Min, J.-K.; Zhou, L.-L.; He, C.-B. Speed-induced extensibility elastomers with good resilience and high toughness. *Macromolecules* **2021**, 54, 3358–3365.
26. Davidson, J.R.; Krebs, H.I. An electrorheological fluid actuator for rehabilitation robotics. *IEEE-ASME T. Mech.* **2018**, 23, 2156–2167.
27. Gao, L.-X.; Zhao, X.-P. Electrorheological behaviors of barium titanate/gelatin composite hydrogel elastomers. *J. Appl. Polym. Sci.* **2004**, 94, 2517–2521.
28. Gao, L.-X.; Liu, Q.-P.; Gao, Z.-W.; Lin, Y. Preparation and characterization of polyimide/silica-barium titanate nanocomposites. *Polym. Composite.* **2008**, 29, 1160–1164.
29. Yin, J.-B.; Zhao, X.-P. Preparation and electrorheological characteristic of Y-doped $BaTiO_3$ suspension under dc electric field. *J. Solid State Chem.* **2004**, 177, 3650–3659.
30. Liu, B.; Shaw, M.T. Electrorheology of filled silicone elastomers. *J. Rheol.* **2001**, 45, 641–657.
31. Liu, B.; Shaw, M.T. Electrorheological effects of ER gels containing iron particles. *J. Intel. Mat. Syst. Str.* **2001**, 12, 57–63.
32. Mitsumata, T.; Sugitani, K.; Koyama, K. Electrorheological response of swollen silicone gels containing barium titanate. *Polymer* **2004**, 45, 3811–3817.
33. Kosińska-Klähn, M.; John, Ł.; Drag-Jarzabek, A.; Utko, J.; Petrus, R.; Jerzykiewicz, L.B.; Sobota, P. Transformation of barium–titanium chloro–alkoxide compound to $BaTiO_3$ nanoparticles by $BaCl_2$ elimination. *Inorg. Chem.* **2014**, 53, 1630–1636.
34. Mao, Y.-P.; Mao, S.-Y.; Ye, Z.-G.; Xie, Z.-X.; Zheng, L.-S. Size-dependences of the dielectric and ferroelectric properties of $BaTiO_3$/polyvinylidene fluoride nanocomposites. *Mater. Chem. Phys.* **2010**, 108, 014102.
35. Huang, K.C.; Huang, T.C.; Hsieh, W.F. Morphology-controlled synthesis of barium titanate nanostructures. *Inorg. Chem.* **2009**, 48, 9180–9184.
36. Merz, W.J. The electric and optical behavior of $BaTiO_3$ single-domain crystals. *Phys. Rev.* **1949**, 76, 1221–1225.
37. Gao, S.-J. Dielectric properties and synthesis of magnesium doped strontium titanate with annona squamosa-like. *Results Phys.* **2020**, 3, 102884.
38. Wu, X.-N.; Gao, L.-X.; Liu, Y.; Gao, Z.-W.; Pei, C.-P.; Gao, S.-J. Preparation and electric field response behavior of barium strontium titanate with different controlled shapes. *Chem. J. Chin. Uni.* **2009**, 30, 1066–1070.
39. He, L.; Gao, L.-X.; Gao, Z.-W.; Zhang, Y.; Wu, X.-N.; Ni, Y.-R. Synthesis and electric field response behavior of 4-Chlorophthalate titanocene complexes. *Chem. J. Chinese U.* **2009**, 30, 855–861.
40. Liu, Q.-P.; Gao, L.-X.; Gao, Z.-W.; Yang, L. Preparation and characterization of polyimide/silica nanocomposite spheres. *Mater. Lett.* **2007**, 61, 4456–4458.
41. Zhang, J.; Sun, L.-D.; Yin, J.-L.; Su, H.-L.; Liao, C.-S.; Yan, C.-H. Control of ZnO morphology via a simple solution route. *Chem. Mater.* **2002**, 14, 4172–4177.
42. Hirata, T.; Ishioka, K.; Kitajima, M. Vibrational Spectroscopy and X-Ray Diffraction of Perovskite Compounds $Sr_{1-x}M_xTiO_3$ (M = Ca, Mg; $0 \le x \le 1$). *J. Solid State Chem.* **1996**, 124, 353–359.
43. Noesges, B.A.; Lee, D.; Lee, J.W.; Eom, C.B.; Brillson, L.J. Nanoscale interplay of native point defects near Sr-deficient Sr_xTiO_3/$SrTiO_3$ interfaces. *J. Vac. Sci. Technol. A* **2022**, 40, 043201.
44. Zvanut, M.E.; Jeddy, S.; Towett, E.; Janowski, G.M.; Brooks, C.; Schlom, D. An annealing study of an oxygen vacancy related defect in $SrTiO_3$ substrates. *J. Appl. Phys.* **2008**, 104, 064122.
45. Naidu, K.C.B.; Sarmash, T.S.; Maddaiah, M.; Reddy, P.S.; Subbarao, T. Synthesis and characterization of MgO doped $SrTiO_3$ ceramics. *J. Aust. Ceram. Soc.* **2016**, 52, 95–101.
46. Jeon, J.E.; Han, H.S.; Park, K.R.; Hong, Y.R.; Shim, K.B.; Mhin, S. The effect of pH control on synthesis of Sr doped barium titanate nanopowder by oxalate precipitation method. *Ceram. Int.* **2018**, 44, 1420–4.
47. Wang, B.-X.; Zhao, Y.; Zhao, X.-P. The wettability, size effect and electrorheological activity of modified titanium oxide nanoparticles. *Colloid Surface. A.* **2007**, 295, 27–33.
48. McHale, G.; Shirtcliffe, N.J.; Newton, M.I. Contact-angle hysteresis on super-hydrophobic surfaces. *Langmuir* **2004**, 20, 10146–10149.
49. Yin, J.-B.; He, L.; Gao, Z.-W.; Gao, L.-X.; Wang, B. Facile method for fabricating titania spheres for chromatographic packing. *Mater. Lett.* **2009**, 63, 2191–2193.
50. Yin, J.-B.; Zhao, X.-P. Electrorheological properties of titanate nanotube suspensions. *Colloid Surface. A.* **2008**, 329, 153–160.
51. Krause, S.; Bohon, K. Electromechanical response of electrorheological fluids and poly (dimethylsiloxane) networks. *Macromolecules* **2001**, 34, 7179–7189.

 doi:10.20944/preprints202406.0849.v1

52. See, H.; Sakurai, R.; Saito, T.; Asai, S.; Sumita, M. Relationship between electric current and matrix modulus in electrorheological elastomers. *J. Electrostat.* **2001**, 50, 303–312.
53. Wang, Y.-F.; Lin, M.-H.; Dai, W.-Q.; Zhou, Y.-W.; Xie, Z.-Y.; Liu, K.-Q.; Gao, L.-X. Enhancement of Fe(III) to electro-response of starch hydrogel. *Colloid Polym. Sci.* **2020**, 298, 1533–1541.